Experimental and Theoretical Aerodynamics of a Sphere in Engineering Education

Etsuo Morishita and Toshiki Homma
Department of Mechanical Engineering, School of Science and Engineering, Meisei University
etsuo.morishita@meisei-u.ac.jp

Introduction

A circular cylinder and sphere are major subjects in the fields of aerodynamics and fluid dynamics. Potential flow around a circular cylinder is widely taught and the lift is explained by the circulation around a circular cylinder. The subject is extended to Joukowsky aerofoil via conformal mapping. The velocities and pressure around the aerofoil are calculated analytically, and therefore, they are very important although numerical solutions are readily available. The same is true for a sphere in the low Reynolds number flows. An exact analytical solution is obtained for the problem, i.e. the Stokes sphere.

The experiments on the aerodynamic drag on circular cylinders and spheres are also classical subjects and are well documented (Vennard and Street, 1982). The drag coefficients of these bluff bodies are important not only in engineering applications but also in sports aerodynamics (Kundu and Cohen, 2004). Critical velocity and unsteady vortex shedding cause varieties of the flight path in football, volleyball, tennis, baseball, golf ball, ping pong, and so on.

In this paper, several aerodynamic experiments conducted during the course of the fluid dynamics project for engineering students to enhance their intuitive and direct understanding of aerodynamic forces are described. Aerodynamics education often tends to be too abstract and many students are lost in the mathematical equations. The drag measurements of a sphere by the balance are explained, together with the pendulum method where the students can visibly experience the force. The Magnus effect is demonstrated by the free fall of a spinning ping-pong ball. Further, the lift of the spinning ping-pong ball pasted at the tip of a miniature motor is measured to quantify the Magnus effect. For the analytical approach, the Stokes sphere spinning around the axis parallel to the uniform flow is studied; circular flow may be added without changes in the original solution. It is an important insight for the engineering students that a potential circulation can be superimposed to viscous flow solutions.

Drag measurement

One of the simplest techniques for measuring the aerodynamic drag of a sphere is shown in Fig.1, where a and b are the arm lengths of the bar, D is the drag, g is the gravitational acceleration, m is the mass of the sphere $(mg > D)$, T is the tension of the string, V is the uniform velocity, and the suffix 0 indicates the initial condition. A low-speed wind tunnel with a vertical exit (300 mm x 300 mm) is used to provide an upward flow in Fig.1. The exit velocity is controlled by a frequency inverter KVFS237, Kasuga E.K. Ltd. for 200 V 50 Hz. Initially, the mass of the sphere is balanced by a stationary mass $(> m)$ on an electronic scale, and the scale is set to zero. The drag of the sphere is measured as a reduction of the tension $T_0 - T$, which is equal to the reading of the scale when $a = b$.

Another intuitive method to measure the aerodynamic drag of a sphere is using a pendulum, as shown in Fig. 2. The drag can be calculated as

$$D = mg \tan\theta ,$$

where F is the resultant force, l is the length of the string, s is the horizontal displacement,

and θ is the angle of the pendulum. Figure 3 shows the results of a softball with a diameter $d = 90\ \mathrm{mm}$ using the pendulum method. The drag coefficient about $C_D \approx 0.6$ is obtained, which is slightly higher compared to that of a magnetically suspended smooth sphere (Sawada, 2014; Okuizumi, Sawada, Nagaike, Konishi, and Obayashi, 2018). The drag measured using the balance in Fig. 1 provides similar but slightly higher values owing to the excessive drag of the support, and the drag coefficient at the low Reynolds number Re based on the diameter becomes smaller and seems to be erroneous. The accurate drag prediction also needs wind-tunnel wall correction (Brown and Lawler, 2003).

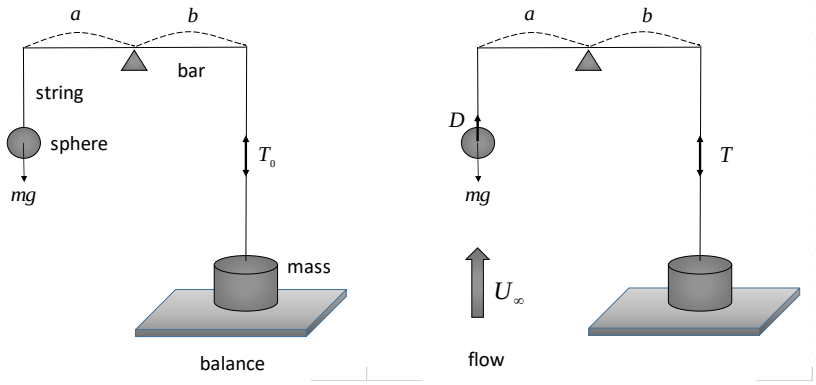

Figure 1: Drag measurement of a sphere using a simple balance

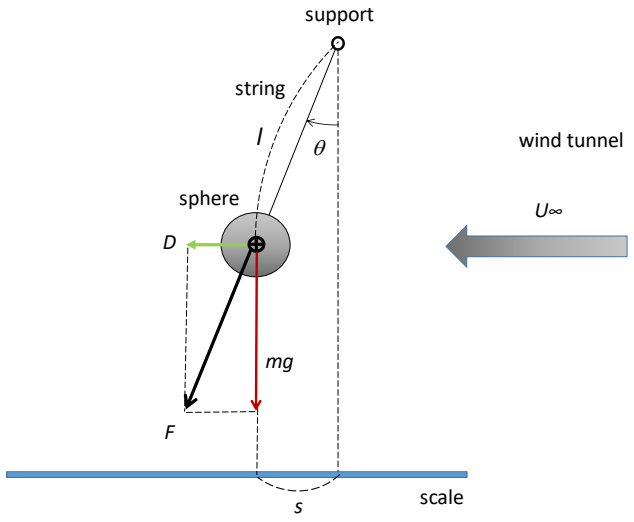

Figure 2: Drag measurement of a sphere using a pendulum

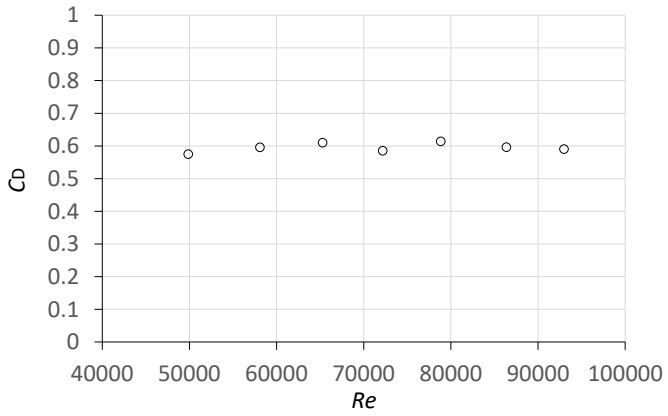

Figure 3: Drag coefficient of softball $d = 90\ \mathrm{mm}$ using the pendulum method

Magnus effect

Aerodynamic force on a spinning ball causes a lateral movement, called the Magnus effect, which is often observed in various ball sports, i.e. baseball, volley ball, football, tennis, and ping-pong (Kundu and Cohen, 2004). In aerodynamics education, a circular cylinder with a circulation Γ is analyzed by the potential flow theory and the lift is obtained using the Kutta–Joukowsky theorem. However, the theoretical expression for a spinning sphere is not available due to the complexity of the flow structure although there are numerous numerical and experimental studies. The Magnus effect experiments are reported by Alaways and Hubbard (2001), and Sareen, Zhao, Sheridan, Hourigan, Thompson, and Jacono (2016). A detailed numerical study is provided by Muto, Watanabe, Tsubokura, and Oshima (2011). The Magnus effect is summarized as a function of the spin ratio, although the results are diverse due to the wide range of the Reynolds number.

A free fall experiment with a ping-pong ball of diameter $d = 40\ \mathrm{mm}$ and mass $m = 2.2\ \mathrm{g}$ is shown in Fig. 4. The ball falls straight downwards without spin; however, it turns either right and left depending on the direction of the rotation. This experiment is effective to demonstrate the Magnus effect because the deflection in the orbit is quite visible owing to the small mass of the ball.

Flow visualization is an indispensable tool in aerodynamics education, and Fig. 5 shows the flow around a spinning sphere with $a\omega / U_\infty \approx 2$ and $Re \approx 1.1 \times 10^4$.

Further, it is interesting to measure the lift of a spinning ping-pong ball attached on a small balance as shown in Fig. 6. A ping-pong ball with a diameter $d = 40\ \mathrm{mm}$ and the mass $m = 2.2\ \mathrm{g}$ is taped at the tip of the shaft of a small model electric motor and the corner flow U_∞ from a 600 mm x 600 mm low speed wind tunnel is blown to the ball. In this experiment, students can experience the lift owing to the spin directly in the unit of gram-force from the digital readings of the electronic balance as shown in Fig. 6, which is otherwise given as a voltage from the amplifier. Figure 7 shows the summary of the experiment at the Reynolds number $Re \approx 1.9 \times 10^4$ in the non-dimensional forms, where C_L is the lift coefficient, C_P is the overall power coefficient, C_Q is the apparent torque coefficient based on the motor input power P, L is the lift, q is the dynamic pressure, $r\,(=a)$ is the radius $(=d/2)$, S is the cross-sectional area of the ping-pong ball, and $C_L = L/(qS)$, $C_P = P/(qSV_\infty)$ and $C_Q = T/(qSr)$.

A six-component balance is used to measure the aerodynamic forces of a spinning ball. The unsteady aerodynamic forces are also measured.

A baseball with inner sensors named MA-Q by Mizuno, Ltd., Tokyo (2019) was used to measure the average ball speed, ball rotation, and inclination of the axis of rotation from the horizon. Some of the output from the baseball to a cellular phone is listed as a spreadsheet format in Table 1. Therefore, the pitcher could modify and improve his own throws from these measurements, i.e. the ball speed and the rotation for example.

Table 1: Baseball sensor output

year	month	day	time	pitcher	arm	throw	type of pitch	ball speed (km/h)	ball rpm	ball inclination (deg.)	comments
2019	7	6	11:07	S	right-handed	three-quarter	straight(four-seam)	100.7	1471	-	
2019	7	6	11:11	S	right-handed	three-quarter	straight	100.4	1376	9	
2019	7	6	11:24	S	right-handed	three-quarter	two-seam	99.1	1359	34	
2019	7	6	11:19	S	right-handed	three-quarter	two-seam	97.1	1207	10	
2019	7	6	11:23	S	right-handed	three-quarter	two-seam	96.8	1324	11	
2019	7	6	11:23	S	right-handed	three-quarter	two-seam	95.9	1408	43	
2019	7	6	11:22	S	right-handed	three-quarter	two-seam	93.8	1179	9	
2019	7	6	11:26	S	right-handed	three-quarter	two-seam	89.9	1224	12	two-seam (variation)
2019	7	6	11:29	F	right-handed	three-quarter	two-seam	79.6	1409	25	
2019	7	6	11:09	F	right-handed	three-quarter	straight(four-seam)	79.5	1369	45	
2019	7	6	11:27	F	right-handed	three-quarter	two-seam	79	1255	14	
2019	7	6	11:21	F	right-handed	three-quarter	two-seam	78.1	1078	36	
2019	7	6	11:28	F	right-handed	three-quarter	two-seam	77.7	1369	16	curve

Figure 4: Free fall of a spinning ping-pong ball along the vertical lope

Figure 5: Visualized Magnus effect ($a\omega / U_\infty \approx 2 \quad Re \approx 1.1\times10^4$)

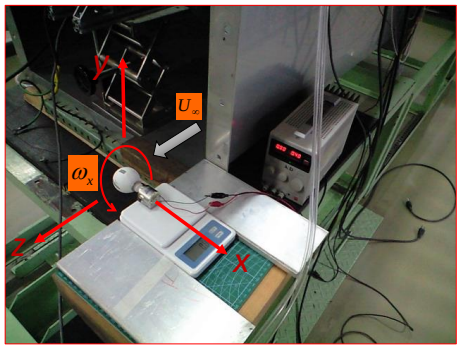

Figure 6: Spinning ping-pong ball on an electronic balance

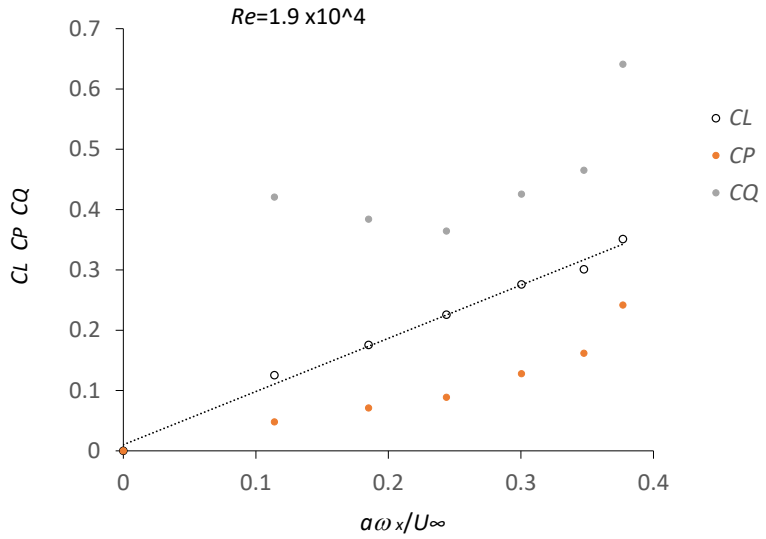

Figure 7: Magnus effect

Analytical solution for a Stokes sphere slowly spinning around the *z*-axis

The axisymmetric Stokes solution for a sphere at very low Reynolds numbers is known (Panton, 1984; Warsi, 1999). The radial and polar velocity components u_r and u_θ together with the stream function ψ are expressed in closed analytical forms. The velocity and stream lines are functions of r and θ, where r is the radial coordinate and θ is the polar angle. The drag coefficient $C_D = 24/Re$ is obtained, where Re is the Reynolds number based on the diameter of the sphere.

We may consider the situation that the Stokes sphere spins slowly at a constant angular velocity ω_z around the *z*-axis parallel to the uniform flow. In the (r,θ,ϕ) spherical coordinate, we can assume that the azimuthal derivative is zero, i.e. $\partial/\partial\phi = 0$, while the velocity component in the same direction exists.

The continuity and momentum equations in the r - and θ - directions are assumed to be the same as the original calculation because of the very low spinning rate. Then, the stream function and velocities remain unchanged and the Stokes solution is applied. The momentum equation in the ϕ -direction becomes

$$\left[\frac{1}{r^2}\frac{\partial}{\partial r}\left(r^2\frac{\partial}{\partial r}\right)+\frac{1}{r^2\sin\theta}\frac{\partial}{\partial\theta}\left(\sin\theta\frac{\partial}{\partial\theta}\right)\right]u_\phi-\frac{u_\phi}{r^2\sin^2\theta}=0\,, \tag{1}$$

where the inertia terms are neglected (Goldstein, 1965). Equation (1) is independent from the viscosity and one of the possible and simple solutions could be a free vortex

$$u_\phi = a^2\omega_z\frac{\sin\theta}{r}\,, \tag{2}$$

where $a^2\omega_z$ is a constant determined from the boundary condition on the surface of the sphere $u_\phi|_{r=a} = a\sin\theta\cdot\omega_z$. Equation (2) is superimposed to the Stokes solution. A similar superposition of the free vortex to the buoyancy viscous pipe flow is shown to simulate a thermal whirl (Morishita, Kumagai, Onodera, Kubota, Moriyama, and Yamazaki, 2018).

Some of the stresses on the sphere are $\tau_{\theta\phi} = 0$, and

$$\tau_{r\phi} = \mu\left(\frac{\partial u_\phi}{\partial r}+\frac{1}{r\sin\theta}\frac{\partial u_r}{\partial\phi}-\frac{u_\phi}{r}\right)\Big|_{r=a} = -2\mu\omega_z\sin\theta\ . \tag{3}$$

The torque T around the *z*-axis becomes

$$T = \int_0^\pi \left(-\tau_{r\phi}\right)\cdot\left(2\pi a\sin\theta\cdot a d\theta\right)\times a\sin\theta = \frac{16}{3}\pi a^3\mu\omega_z\ . \tag{4}$$

The torque coefficient C_Q is obtained as

$$C_Q \equiv \frac{T}{\frac{1}{2}\rho U_\infty^2\cdot\pi a^2\cdot a} = \frac{1}{3}\frac{64}{Re}\left(\frac{a\omega_z}{U_\infty}\right). \tag{5}$$

Figures 8 (a) and (b) with the coordinate illustration show the path-lines on the stream tube at $a\omega_z/U_\infty = 1$ with $\psi/\left(a^2U_\infty\right) \approx 0.011$ and 0.113, respectively (Mathematica 2018). The stream tube is not affected by the spin around the z -axis by the present assumption.

The flow moves upwards, i.e. to the positive *z*-direction. The rotation of the sphere is noticeable near the surface, see Fig.8. It is useful for the engineering students to find that the potential circulation can be added to the Stokes flow which remains unchanged in spite of the rotation. The similar vortex superposition might be possible to the Hagen-Poiseuille flow which is an indispensable subject in the aerodynamics education.

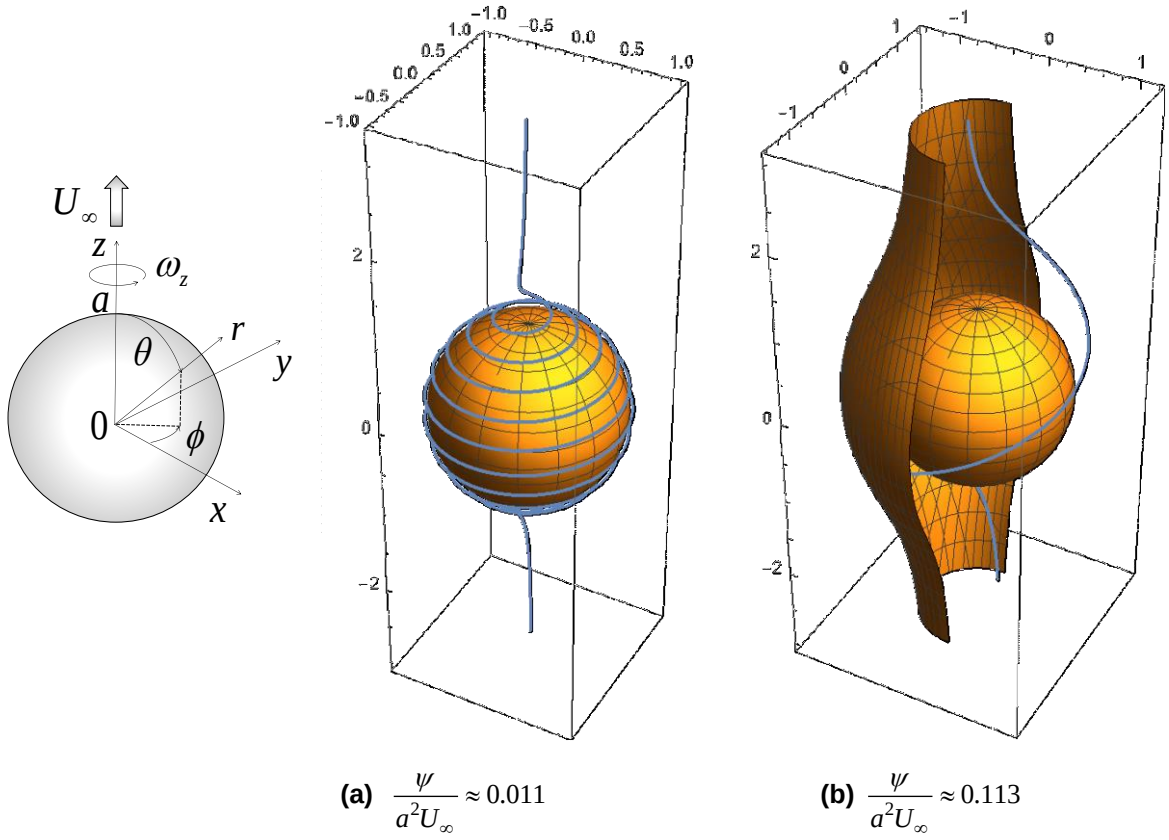

Figure 8: Path-lines on the stream tube around a sphere $r/a=1$ **spinning at** $a\omega_z/U_\infty=1$

Concluding Remarks

Several experimental problems and an analytical example of aerodynamics of a sphere are used as engineering education tools. A simple mechanical balance and a pendulum are introduced to measure the drag of a sphere. Hands-on drag measurements in the units of gram-force are very useful for engineering students to understand the degree of aerodynamic forces and the converted drag coefficient. Although the drag coefficients in the laboratory are the same as those of aircrafts and cars, the values of drag range from grams to tons. Magnus effect is often observed in the daily sports event, and it is valuable to observe the visualized flow around a spinning sphere how the lift is generated. The lift by the Magnus effect is easily demonstrated by a spinning ball on the miniature electronic scale. A slowly spinning Stokes sphere around the axis parallel to the uniform flow is solved analytically, which has the same stream tube as the original solution despite the rotation. Although the vortex superposition is limited to the creeping flows, it might be useful for the engineering students to find that a free vortex can be superimposed to the original viscous flow solution.

References

Alaways, L. and Hubbard, M. (2001). Experimental determination of baseball spin and lift. *Journal of Sports Science*, 19, 349-358.

Brown, P.P. and Lawler, D.F. (2003). Sphere drag and settling velocity revisited. *Journal of Environmental Engineering*, ASCE, Mar. 2003, 222-231.

Goldstein, S. (1965). *Modern developments in fluid dynamics*, Vol.1 (pp104-105). New York: Dover.

Kundu, K. K. and Cohen, I.M. (2004). *Fluid mechanics*, 3rd edition (pp.353-358). Elsevier Academic Press: Amsterdam.

MA-Q (2019), https://www.mizuno.jp/baseball/products/MAQ/ (in Japanese), Mizuno, Tokyo.

Morishita, E., Kumagai, I., Onodera, K., Kubota, R. Moriyama, Y. and Yamazaki, T. (2018). *A mathematical model for a laminar spiral flow to approximate fire whirl*. Paper presented at the 10th International Conference Engineering Computational Technology 2018, Sitges, Barcelona, Spain.

Muto, M., Watanabe, H., Tsubokura, M. and Oshima, N. (2011). Negative Magnus effect on a rotating sphere at around the critical Reynolds number. *Journal of Physics. Conference Series* 318, 032021.

Okuizumi, H., Sawada, H., Nagaike, H., Konishi, Y. and Obayashi, S. (2018). *Introduction of 1-m MSBS in Tohoku University, New device for aerodynamics measurements of the sports equipment*. Paper presented at the 12th Conference of the International Sports Engineering Association, Brisbane, Queensland, Australia.

Panton, R. L. (1984). *Incompressible flow* (pp.644-657). New York: John Wiley & Sons.

Sareen, A., Zhao, J., Sheridan, J., Hourigan, K. Thompson, M. and Jacono, D.L. (2016). *Flow past a transversely rotating sphere*. Paper presented at the 11th International Conference on Flow-induced vibrations, The Hague, The Netherlands.

Sawada, H. (2014). Wind tunnels with magnetic suspension and balance system. *Nagare*, 33, 267-272.

Vennard, J.K. and Street, R.K. (1982). *Elementary fluid mechanics* 6th edition (pp.628-634). New York: John Wiley & Sons.

Warsi, Z.U.A. (1999). *Fluid dynamics: Theoretical and computational approach*, second edition (pp.238-243). Boca Raton: CRC Press.

Wolfram Research Inc., (2018). Mathematica, Version 11.3, Champaign, IL.

Acknowledgement

We would like to thank Editage (www.editage.com) for English language editing.